Q. J. R. Meteorol. Soc. (1998), **124**, pp. 101–122

Aircraft observations of the surface energy balance in TOGA-COARE

By A. L. M. GRANT[1]* and P. HIGNETT[2]
[1]*Hadley Centre for Climate Prediction and Research, UK*
[2]*Meteorological Office, UK.*

(Received 3 June 1996 ; revised 30 April 1997)

SUMMARY

The TOGA-COARE (Tropical Ocean/Global Atmosphere Coupled Ocean–Atmosphere Response Experiment) was an international observational campaign designed to study the processes that occur in the Pacific warm pool region. Data from the Meteorological Research Flight C130 aircraft are presented to illustrate some of the characteristics of the surface energy balance in this region. The dominant terms in the balance are the turbulent latent-heat flux and the solar flux. The C130 moisture flux data are compared with a parametrization based on data from the *RV Moana Wave*, one of the ships that took part in the COARE. It is found that there is no evidence for a systematic difference between the aircraft and ship flux estimates. In addition to the comparison with the COARE parametrization the effect of gustiness due to convective clouds on the surface latent-heat flux is estimated for three flights, and the thermal balance of the mixed layer in undisturbed conditions described. The data suggest that direct solar absorption is an important part of the thermal balance, and the implications for diurnal variations in the mixed-layer temperature are considered.

The variation in the downwelling solar flux with cloud cover is compared with simple parametrizations, which are found to agree reasonably well with the present data. The correlation between the long-wave and short-wave cloud forcings at the surface are described, to illustrate the different effects of different cloud types on the surface radiative balance.

KEYWORDS: Cloud forcing Convective gustiness Surface fluxes

1. INTRODUCTION

The role of the tropical oceans in determining the character of the general circulation and climate has long been recognised. The coupling between the ocean and atmosphere occurs through momentum and energy fluxes at the air–sea interface. To achieve reasonable results from coupled ocean–atmosphere models the representation of the surface energy balance and momentum transfer is of crucial importance.

The Tropical Ocean/Global Atmosphere Coupled Ocean–Atmosphere Response Experiment (TOGA-COARE) was designed to study the processes occuring in the Pacific warm pool region. The surface energy balance of this region is not well understood from observations (Webster and Lukas 1992), and ocean models forced with atmospheric flux fields, within the range of uncertainty of the available observations, give significantly different sea surface temperatures (Gordon and Corry 1991). The interfacial subprogram of the TOGA-COARE was intended to study the surface energy exchanges to improve the parametrization of the surface energy balance.

Fairall *et al.* (1996) have described a bulk parametrization scheme for the surface fluxes of momentum, moisture and sensible heat (which will be referred to as the COARE algorithm). The parametrization of the turbulent fluxes is based on the model described by Liu *et al.* (1979). The algorithm also includes parametrizations for the cool skin effect and the warming of the upper ocean by the absorption of solar radiation. One aspect of this parametrization is the careful specification of geophysical constants and thermodynamic relationships (e.g. the dependence of the latent heat of vaporization on temperature) that are used. However, the accuracy of the parametrization ultimately depends on the accuracy of the measurements used to tune the scheme. The scheme described by Fairall *et al.* (1996) was tuned to data obtained by the *RV Moana Wave* during the TOGA-COARE. The *Moana Wave* was one of a number of ships and aircraft which took part in the TOGA-COARE

* Corresponding author: Hadley Centre for Climate Prediction and Research, Meteorological Office, London Road, Bracknell, Berkshire, RG12 2SY, UK. e-mail: almgrant@meto.gov.uk.

that were equipped with instrumentation for measuring turbulent fluxes. As flux data from these other platforms become available it is expected that they will be used to test the COARE algorithm and possibly lead to revisions.

Fairall *et al.* (1996) compared eddy correlation fluxes from the National Center for Atmospheric Research (NCAR) Electra aircraft with estimates from the COARE algorithm. The bulk estimates were on average 7% larger than the eddy correlation fluxes, although the scatter in the fluxes was large. Zhang and Grossman (1996) have compared the COARE algorithm with eddy fluxes measured during the Central Equatorial Pacific Experiment (CEPEX) (which took place immediately after the TOGA-COARE) by one of the National Oceanic and Atmospheric Administration (NOAA) P3 aircraft that also took part in the TOGA-COARE, and found that the eddy correlation fluxes were about 14% larger than those calculated from the scheme. The differences between the eddy-correlation fluxes and those calculated from the COARE algorithm arise from systematic errors in the mean measurements of the aircraft relative to the ships as well as possible systematic errors in the eddy fluxes, and it is important that they are resolved.

Many intercomparisons between the different flux measuring platforms were carried out during the TOGA-COARE, and the results from these are being assessed (Bradley and Weller 1995). However, direct comparison of fluxes measured by ships and aircraft is made difficult by their different sampling strategies. Typically, to obtain statistically reliable flux estimates, shipborne measurements require averaging times of 30–60 minutes. Aircraft, in contrast, require averaging distances of 20–30 km (approximately 5 minutes flying time). Because of this difference in sampling strategies, a more indirect comparison using the COARE algorithm is useful in determining the accuracy with which the turbulent fluxes in the surface energy balance can be parametrized. This is also important if data from the different platforms deployed for the TOGA-COARE are to be combined, to study the spatial and temporal variability of surface fluxes in the COARE domain and the response of the ocean to this varying forcing.

The UK Metorological Office Meteorological Research Flight (MRF) C130 was one of the instrumented aircraft that took part in the TOGA-COARE. This paper presents some of the features of the surface energy balance observed during seven flights in the COARE Intensive Flux Array (IFA). In the following sections the turbulent and radiative components of the energy balance will be considered separately; because of their magnitude and variability the latent-heat and solar fluxes are emphasized, but the other fluxes are also considered.

2. Instrumentation and data processing

(*a*) *Experiment details*

During January 1993 the MRF C130 aircraft (hereafter C130) carried out seven flights in the TOGA-COARE IFA, centred on 2°S and 156°E. Each flight consisted of a number of horizontal runs, approximately 150 km long. Low-level runs were carried out at altitudes of 30 m or 60 m above the surface, with higher-level runs made in the upper half of the boundary layer. Interspersed with the horizontal runs was a series of profiles extending to about 1500 m. Deeper profiles, between the surface and 6 km, were carried out at the beginning and end of each flight, when conditions were suitable. Dates, times and a brief description of the prevailing meteorological conditions for the seven flights used in this study are given in Table 1 (note that local noon was at about 0200 UTC).

The C130 is instrumented to make fast-response measurements of the three wind components, temperature and humidity, which can be used to estimate turbulent fluxes by the eddy-correlation technique. In addition, measurements of incoming and outgoing

TABLE 1. DESCRIPTION OF C130 FLIGHTS.

Flight Number	Date (ddmmyy)	Time (UTC)	Conditions
A224	180193	0001–0503	Convection with precipitating Cu
A225	190193	0100–0530	Convection with precipitating Cu
A227	230193	0030–0500	Patchy small Cu, otherwise clear
A228	240193	0001–0400	Patchy small Cu, otherwise clear
A229	250193	0001–0400	No low cloud, Cirrus cover
A232	300193	0001–0230	Convection with precipitating Cu
A233	310193	2330(3001)–0300	Overcast, stratiform cloud

TABLE 2. ACCURACIES FOR METEOROLOGICAL PARAMETERS.

Quantity	Instrument	Accuracy
Air temperature	Platinum resistance thermometer.	±0.3 degC
Dew-point	Mirror hygrometer	±0.3 degC
Sea surface temperature	Radiometer	±0.3 degC
Horizontal wind components	Pitot system + INS	±0.4 m s^{-1}
Short-wave radiation	Pyranometer	±3%
Long-wave radiation	Pyrgeometer	±10 W m^{-2}

solar and long-wave radiation, and radiometric sea surface temperature were made. The basic instrumentation on the C130 is described by Nicholls (1978), but there has been a number of changes made in both the instrumentation and processing over the years, so a brief description relevant to the TOGA-COARE is given here.

Wind components were measured using a gust probe mounted ahead of the aircraft on a 7 m rigid boom. The gust probe consists of a pitot-static probe, angle-of-attack and angle-of-sideslip vanes. The aircraft motion and attitude were determined by an inertial navigation system (INS), mounted at the base of the boom. Drifts in the INS horizontal ground speed components were corrected by reference to Omega and Global Positioning System navaids. Because of resonances in the tubing of the pitot-static system, accurate measurement of wind fluctuations is limited to frequencies below 3 Hz. However, the effect on the vertical-velocity measurements is small and there is little effect on turbulent flux estimates.

It is difficult to assess the absolute accuracy of the aircraft wind speeds needed to estimate the uncertainty in the transfer coefficients derived below. The main source of error is caused by drifts in the INS, which is reflected in the figure quoted in Table 2. However, these are time dependent and vary from flight to flight, so that combining data from a number of flights should reduce them. Other errors in the wind finding system (e.g. errors in airspeed) lead to heading-related errors in the winds, and these may be reduced by averaging data from different flights when different headings were used. From calibration manoeuvres, errors in the true airspeed may lead to wind errors of ±0.2 m s^{-1}. For the present calculations this will be taken as an estimate of the absolute accuracy of the wind finding system, since it would be difficult to detect smaller errors.

Temperature was measured with a platinum-resistance thermometer in a Rosemount reverse-flow housing, mounted on the boom behind the gust probe. The measured temperature was corrected for kinetic heating effects, using the measured true airspeed and

an empirically determined recovery factor. A further correction was made to account for the response of the thermometer, using the technique described by McCarthy (1973). This correction increased eddy-correlation estimates of the sensible-heat fluxes obtained on low-level runs by about 15%.

Low frequency fluctuations in humidity were measured by a General Eastern dew-point hygrometer. Because the response of this instrument is not adequate for estimating turbulent fluxes, a Lyman-α humidiometer was used to measure high frequency fluctuations of the absolute humidity. The Lyman-α probe is part of the C130 total water content probe which is described by Nicholls *et al.* (1990). The Lyman-α probe is subject to drifts and was, therefore, calibrated in flight against the General Eastern hygrometer (Friehe *et al.* 1986). The sensitivity was determined for each horizontal run by comparing the output of the Lyman-α probe, averaged over five seconds, with the absolute humidity calculated from the General Eastern hygrometer and the temperature of the air in the Lyman-α sample volume. Since there did not appear to be any significant difference between the sensitivities calculated for different flights (the standard deviation of the calculated sensitivies was only 3%) an average value has been used for all flights. The Lyman-α probe is mounted on the airframe close to the base of the boom, approximately 8 m behind the gust probe. To account for this separation a 0.1 second lag was introduced into the Lyman-α data. The inclusion of this time lag increased the humidity fluxes by up to 10% on low-level runs.

Short-wave radiative fluxes were measured using upward and downward facing Eppley PSP pyranometers. The passband of the domes is 0.3 to 3 μm. Corrections to the direct beam flux for aircraft attitude were made using data from the INS. The calibration of the pyranometers and the processing of the data is described by Saunders *et al.* (1992). Long-wave fluxes were measured with upward and downward facing MRF pyrgeometers (Foot 1986), using silicon domes with a passband of 4 to 50 μm.

The radiometric sea surface temperature was measured with a Barnes PRT4 radiometer, which was calibrated during flight by exposing it to a black-body target of known temperature. The sea surface temperature determined from the PRT4 radiometer differs from the temperature required to estimate transfer coefficients, because the emissivity of water is less than one. Reflection of downwelling long-wave radiation from the surface causes the difference between the measured radiative temperature and the true skin temperature to be affected by the presence of cloud above the aircraft (Saunders 1970). For the present data a correction has been made by using an empirical relationship between the zenith sky radiance, in the PRT4 radiometer passband, and the broad band downwelling long-wave radiation measured by the upward facing pyrgeometer. The relationship was derived for a tropical model atmosphere (Ellingson *et al.* 1991) using a medium-resolution radiative-transfer model (MODTRAN, Berk *et al.* 1989). The correction varies from $\approx$0.3 degC under clear skies to $\approx$0 degC under low cloud. Table 2 lists the estimated accuracy of meteorological measurements from the C130.

Turbulent fluxes of momentum, sensible and latent heat were estimated using the eddy-correlation technique. Averages were taken over 25 km segments, with linear trends removed from the segments before the fluxes were calculated. Co-ordinate rotations were not applied to remove the mean vertical velocity over the segments, rather the mean value was subtracted. This was done because, although the mean vertical velocities are relatively large due to the high airspeed, they imply only small angular misalignments (of order 0.2 degrees) between the INS platform and the gust vanes. In areas of deep convection turbulent fluxes were calculated only for those sections of a run not affected by large changes associated with convective outflows. Cospectra show that 25 km was adequate to resolve all of the flux-carrying scales at the altitude of the low-level runs (30 or 60 m above the surface).

The humidity time series showed considerable low frequency variability, which appears to produce significant random variation in the fluxes. To reduce this variability the humidity time series were high-pass filtered, with a cut-off at about 10 km. This filtering reduces the fluxes by about 5%, and the final fluxes were increased by 5% to account for this.

(*b*) *Instrumental biases*

The C130 operated close to the *RV Franklin* on two occasions (flights A228 and A229). These flights provide an opportunity to assess possible biases of the C130 mean data relative to the ships (since intercomparison data from the ships have already been compared to estimate the biases between different ships, Fairall *et al.* (1996)). These biases can be accounted for to reduce systematic differences in the transfer coefficients arising from differences in mean measurements. Comparing mean quantities is somewhat easier than comparing fluxes, because the averaging times required to get reliable estimates are much shorter. For these two flights the sea surface temperature and humidity were quite uniform over the aircraft operating area, the standard deviations being respectively ± 0.1 degC and ± 0.2 g kg^{-1} for 25 km averages.

The sea surface temperatures measured by the C130 on flights A228 and A229 were on average 0.35 degC warmer than the thermosalinograph measurements on the *Franklin*. The thermosalinograph intake on the *Franklin* is 2 m below the surface, and estimates obtained from the COARE algorithm suggest that the skin temperature should be 0.05 degC higher. Because the difference between the *Franklin* and C130 sea surface temperatures is within the expected instrumental accuracy, and also because the PRT4 radiometer is calibrated on a flight by flight basis, no adjustment has been made to the sea surface temperature data used below. Rather, the effect of this difference is incorporated into the estimate of the uncertainty in the calculated transfer coefficients (note that reducing the sea surface temperatures by 0.3 degC would increase the calculated transfer coefficients by 5%).

The humidity measured by the C130 is 0.8 g kg^{-1} lower than the *Franklin* measurements (the difference has been adjusted to account for the different measurement heights). This corresponds to a difference in dew-point of ≈ 0.8 degC. Previous intercomparisons have shown differences of this magnitude between the C130 and ship measurements, as well as in aircraft–aircraft intercomparisons (Nicholls et al. 1983). Although the difference is consistent with the accuracies expected from the kind of instruments used (e.g. Coantic and Friehe 1980; Kaimal 1986) it is still large, and the C130 dew-point data used below have been adjusted. A consequence of increasing the C130 dew-points is to alter the calculated sensitivity of the C130 Lyman-α probe because of the nonlinear relationship between saturated vapour pressure and temperature. An increase in the dew-point of 0.8 degC causes the calculated sensitivity of the Lyman-α to be increased by 4.5%. Overall, increasing the C130 dew-point measurements by 0.8 degC leads to an increase of about 14% in the calculated transfer coefficient for moisture.

Figure 1 shows a plot of $\overline{w\theta}/U$, (w is vertical velocity, θ is potential temperature, $\overline{w\theta}$ is the kinematic heat flux and U is wind speed) against the sea–air temperature difference, $\Delta\theta$, ($\Delta\theta = (\theta_{\text{sea}} - \theta)$). A least-squares regression indicates that $\overline{w\theta}/U$ does not go to zero for $\Delta\theta = 0$, as might be expected, and the data suggest that the measured sea–air temperature difference is low by about 0.6 degC (the estimated error in the intercept is ± 0.2 degC). A comparison between the *Franklin* and C130 air temperatures does not suggest a consistent difference ($T_{\text{C130}} - T_{\text{Fran}} = 0.0$ degC (A228) and 0.5 degC (A229)). Since the sea surface temperatures have been referenced to those from the *Franklin* separately, the air temperatures from the C130 have been reduced by 0.6 degC. A similar consistency check

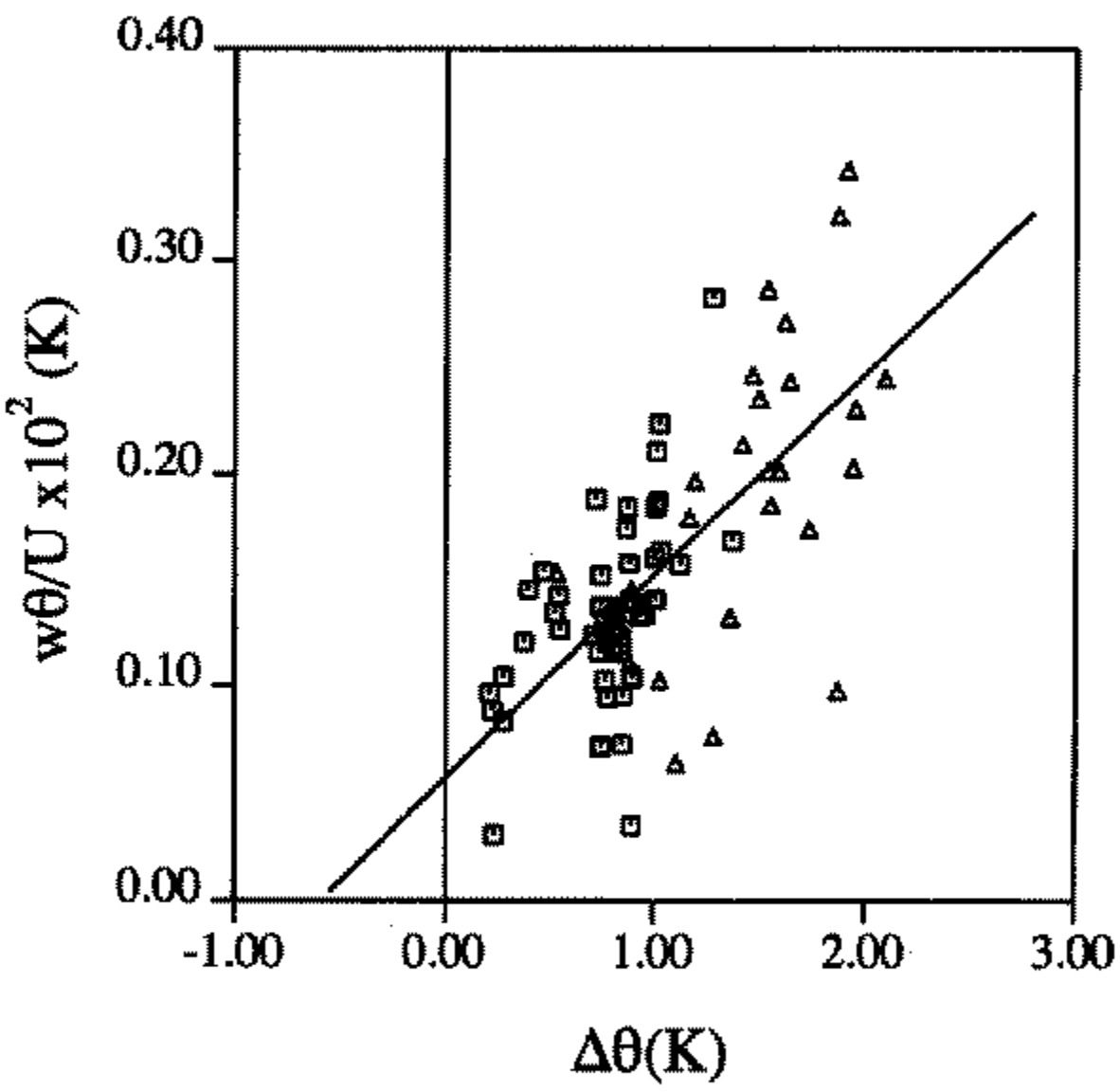

Figure 1. Plot of $\overline{w\theta}/U$ (see text) against the sea–air temperature difference, $\Delta\theta$. The squares denote data from undisturbed flights and the triangles data from flights with convection. The line is a least-squares fit.

is not possible for the moisture flux because the range of air–sea humidity differences is too limited.

A potential source of difference between flux measurements by ship and aircraft unrelated to instrumental inaccuracies, is the height difference. Any vertical gradients in the fluxes would lead to different fluxes being measured. For the flights in undisturbed conditions the flux divergence can be estimated directly from the difference in the fluxes obtained on the high- and low-level runs. For the humidity flux the difference between the flight-level fluxes and the surface flux implied by the observed divergences is about 2%.

3. The surface energy balance

The net energy flux into the ocean is:

$$F_{\text{net}} = (1-\alpha)S^{\downarrow} + (L^{\downarrow} - L^{\uparrow}) - H - \lambda E\,, \tag{1}$$

where: F_{net} is the net flux into the ocean; $S^{\downarrow}$ is the downward solar flux; α is the surface albedo, taken to be 0.06; $L^{\downarrow}$ is the downwelling long-wave radiation; $L^{\uparrow}$ is the upwelling long-wave radiation; H is the turbulent sensible-heat flux; λE is the turbulent latent-heat flux; and λ is the latent heat of vaporization of water.

It is possible to estimate an average over the period of the aircraft flight of each of the terms on the right-hand side of Eq. (1). The long-wave flux and the sensible- and latent-heat fluxes, averaged over each flight, are listed in Table 3; the sign convention is consistent with Eq. (1). The turbulent fluxes, listed for days when deep convection was present, may be biased, since estimates were made only for certain parts of each run. (Note that for convenience all the terms in Eq. (1) are referred to as fluxes, although the radiative terms should more properly be termed irradiances). Although there are diurnal variations in the sea surface temperature, and hence both the long-wave and turbulent fluxes, due to

TABLE 3. AVERAGE OF TERMS IN EQ. (1) OVER EACH FLIGHT.

Flight	$(1-\alpha)S^{\downarrow}$ (W m^{-2})	$L^{\downarrow}-L^{\uparrow}$ (W m^{-2})	H (W m^{-2})	λE (W m^{-2})	F_{net} (W m^{-2})
A224	169	−34	9	61	65
A225	228	−38	15	142	33
A227	300	−62	6	128	104
A228	302	−60	9	161	72
A229	293	−68	9	131	85
A232	192	−37	9	90	56
A233	170	−30	10	153	−23

A positive value of F_{net} implies an energy flux into the ocean

the absorption of solar radiation in the upper part of the ocean, these are relatively smaller than variations in the measured short-wave flux, which depend strongly on the time of day. To allow a more direct comparison with the other fluxes an estimate has been made of the diurnally averaged short-wave flux under unchanged atmospheric conditions, i.e. assuming that the ratio between the observed flux and the calculated clear-sky flux during the measuring period remains constant. Note that this does not constitute an estimate of the actual average flux over a particular day, but the consistency of this can be tested using data from the IMET buoy, moored at 1°45′S, 156°E (Hosom *et al.* 1995), which showed that the daily averaged flux estimated from the measured flux over the four hour period spanning local noon was within ±15% of the observed daily average. The average clear-sky flux for each day was calculated using the radiation model of Edwards and Slingo (1996) using aircraft profiles of temperature and humidity, supplemented above ≈ 6 km by a tropical-model atmosphere (Ellingson *et al.* 1991).

For six of the flights the net flux is into the ocean, with the magnitude varying between 30 W m^{-2} and 100 W m^{-2}. The one day on which there was a net energy loss from the ocean was characterized by overcast conditions with strong winds. For all the days considered, the largest terms in the surface energy budget are the net solar flux and the latent-heat flux. The solar and latent-heat fluxes also show the largest variations between flights and are, between them, responsible for most of the flight to flight variation in the net flux. Variations in the net long-wave flux and the sensible-heat flux are much smaller.

The flight to flight variations in the radiative fluxes are largely due to differences in the cloud cover, whilst the variations in the latent-heat flux are largely related to differences in wind speed. The variation in the latent-heat flux with wind speed is shown in Fig. 2. The flux increases by about 19 W m^{-2} for a 1 m s^{-1} increase in wind speed. A least-squares fit to the the data in Fig. 2 suggests a latent-heat flux of 38 W m^{-2} at zero wind speed and, although the significance of this estimate is not high, it is similar to the flux obtained from the *Moana Wave* for wind speeds less than 0.5 m s^{-1} (Fairall *et al.* 1996). Data obtained in disturbed and undisturbed conditions are distinguished in Fig. 2. There is a tendency for the latent-heat fluxes in disturbed conditions to be slightly lower than the regression suggests, due to a smaller air–sea humidity difference than the average on these occasions.

The variability of the flux estimates on each flight is shown by the error bars in Fig. 2, and appears to be quite large. In part, this arises from variations in conditions over the operating area, but there is a significant contribution from statistical-sampling error. For a 25 km averaging length the estimated sampling error for the humidity flux is 20% (Mann and Lenschow 1994), which is comparable to the observed variability.

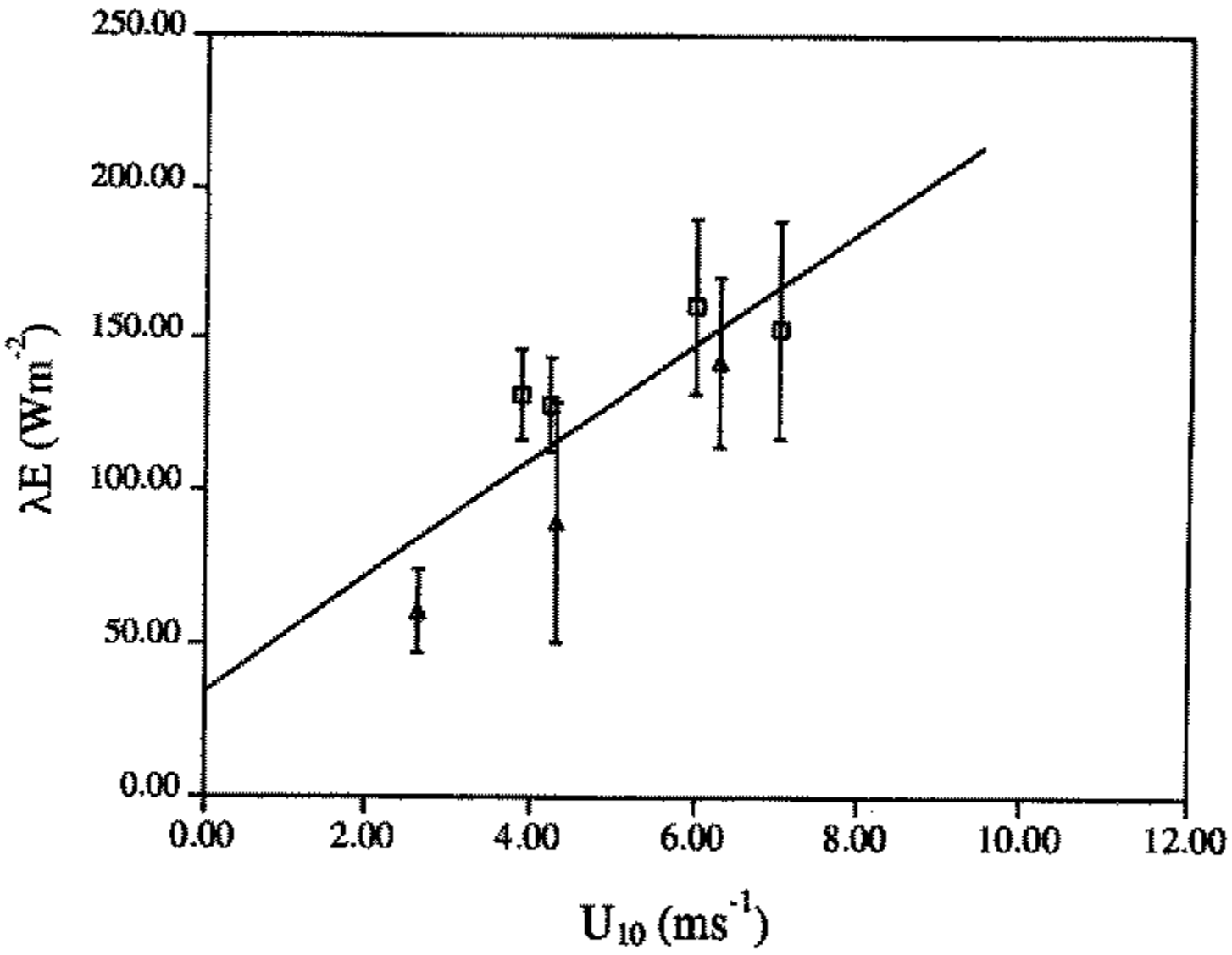

Figure 2. Plot of latent-heat flux, λE, against the 10 m wind speed, u_{10}. The symbols are the same as Fig. 1, and the sloping line is a least-squares fit.

(*a*) *Turbulent fluxes*

The parametrization of surface fluxes in general circulation models (GCMs) is commonly based on Monin–Obukhov similarity theory, with the fluxes given by:

$$\tau = \rho \frac{\kappa^2}{(\kappa / C_{\mathrm{dn}}^{1/2} - \psi_{\mathrm{m}}(z/L))^2} U^2 , \tag{2}$$

$$H = \rho c_p \frac{\kappa C_{\mathrm{d}}^{1/2}}{(\kappa C_{\mathrm{dn}}^{1/2} / C_{\mathrm{hn}} - \psi_{\mathrm{t}}(z/L))} U(\theta_{\mathrm{sea}} - \theta) , \tag{3}$$

$$\lambda E = \lambda \rho \frac{\kappa C_{\mathrm{d}}^{1/2}}{(\kappa C_{\mathrm{dn}}^{1/2} / C_{\mathrm{en}} - \psi_q(z/L))} U(Q_{\mathrm{sea}} - Q) , \tag{4}$$

where: τ is the surface stress; ρ is the air density; z is the height above the surface; c_p is the specific heat at constant pressure; θ and θ_{sea} are potential temperatures of air at height z and at the sea surface, respectively; Q and Q_{sea} are the specific humidities of the air at height z and at the sea surface, respectively; C_{dn}, C_{hn} and C_{en} are neutral-transfer coefficients which depend on height; $\psi_{\mathrm{m}}(z/L)$, $\psi_{\mathrm{t}}(z/L)$ and $\psi_q(z/L)$ are functions of stability; L is the Monin–Obukhov length; and κ is the von Kármán constant. The values of the neutral-transfer coefficients are at the heart of the COARE parametrization. (Note in air–sea interaction studies it is usual to present the neutral-transfer coefficient for a height of 10 m).

The stability functions in Eqs. (2)–(4) have been determined empirically, and there are several formulations in the literature (e.g. Hogstrom 1988). To ensure that the transfer coefficients derived from the C130 data are comparable with those derived from the *Moana Wave* data, the functions used here have been taken from Fairall *et al.* (1996). For small values of z/L these functions follow the standard Businger–Dyer formulation of the non-dimensional gradients, but have been modified to be consistent with the expected free convective behaviour at large $-z/L$. The humidity at the sea surface in Eq. (4) is taken to

be 0.98 of the saturated humidity over pure water at the sea surface temperature, to account for the effect of salinity (Kraus 1972). The saturated vapour pressure over pure water is calculated using Tetens' formula (Buck 1981), as used in the COARE bulk parametrization.

At low wind speeds the eddy-correlation estimates of the shear stress suffer from large sampling errors, and individual estimates can be positive for which a sensible value of the Monin–Obukhov length cannot be obtained. To obtain the neutral-transfer coefficients from the present data, the Monin–Obukhov length appearing in Eqs. (2)–(4) has been calculated using bulk estimates of the fluxes rather than the eddy-correlation fluxes. In terms of the bulk variables the stability parameter is

$$\frac{z}{L} = 10.5 \frac{\theta U^2 z}{g \Delta \theta_v} , \tag{5}$$

where g is the acceleration of gravity, and $\Delta\theta_v$ is the air–sea difference in virtual temperature. The numerical factor of 10.5 has been obtained from the average values of the flight-level transfer coefficients obtained from the present data. In addition, estimates of winds, temperatures and humidities at 10 m were obtained from the flight-level values, using a friction velocity calculated from the flight-level winds and an average value for the drag coefficient.

Figures 3(a)–(c) show the neutral, 10 m transfer coefficients for momentum, sensible- and latent-heat fluxes, plotted against wind speed and compared with the COARE algorithm. The average values of the transfer coefficients derived from the C130 data are:

$$C_{dn} = 1.12 \times 10^{-3}, \tag{6}$$

$$C_{hn} = 0.93 \times 10^{-3}, \tag{7}$$

$$C_{en} = 0.93 \times 10^{-3}. \tag{8}$$

The neutral drag coefficient is consistent with the roughness length specification used in the COARE bulk parametrization, i.e.,

$$z_0 = 0.11\nu/u_* + 0.011u_*^2/g , \tag{9}$$

where ν is the kinematic viscosity of air, and u_* is the surface friction velocity $(\tau^{1/2}/\rho)$. The roughness length specification in the COARE algorithm was tuned to stress estimates derived from dissipation measurements since the direct eddy-correlation estimates were considered uncertain, possibly due to inadequate motion correction. Song *et al.* (1996) have found that eddy-correlation stress estimates from the *RV Kexue #1*, obtained during the TOGA-COARE, are smaller than dissipation and bulk estimates from the COARE algorithm. Given the uncertainties in the shipborne stress measurements, the results in Fig. 3(a) are a useful check on the COARE parametrization using direct eddy-correlation estimates.

The C130 transfer coefficients for heat and moisture are smaller than those from the COARE parametrization over the full range of wind speeds. The COARE algorithm gives $C_{en} = 1.11 \times 10^{-3}$, compared with 0.93×10^{-3} for the C130 data. Since the COARE parametrization has been tuned to data from the *Moana Wave*, this difference between the COARE parametrization and the C130 data might indicate a systematic difference between the ship and aircraft flux data.

Table 4 lists a number of recent estimates of C_{en} obtained over the tropical oceans for wind speeds around 4 m s^{-1} (the value from Tsukamoto and Ishida (1995) has been adjusted to be at 10 m). The values are all lower than the recommended value of 1.2×10^{-3} (Smith 1989), and generally somewhat lower than the COARE value. The present estimate

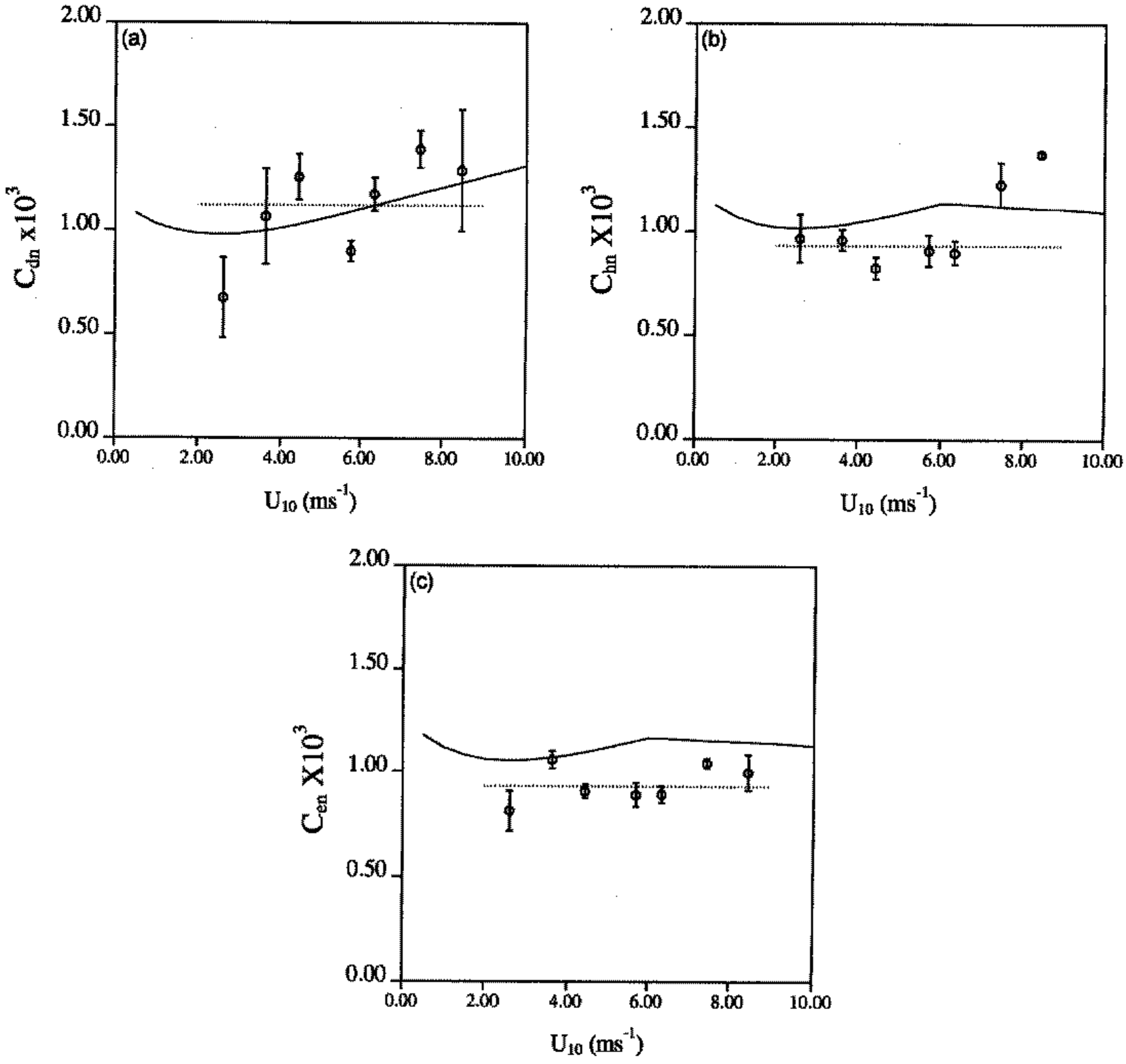

Figure 3. Neutral-transfer coefficients as a function of 10 m wind speed, U_{10}, (a) drag coefficient, C_{dn}, (b) transfer coefficient for heat, C_{hn}, and (c) transfer coefficient for moisture, C_{en}. The full curves are from the COARE bulk parametrization, the dotted lines are the average value of the C130 transfer coefficients.

TABLE 4. PUBLISHED ESTIMATES OF C_{en} OVER TROPICAL OCEANS

Author	$C_{en} \times 10^3$	Platform
Greenhut and Bean (1981)	1.07	Aircraft
Greenhut and Khalsa (1995)	0.94	Aircraft
Bradley *et al.* (1991)	0.89	Ship
Fujitani (1992)	0.94	Ship
Fairall *et al.* (1996)	1.11	Ship/TOGA-COARE
Tsukamoto and Ishida (1995)	1.10	Ship/TOGA-COARE
Present	0.93	Aircraft

of C_{en} is towards the lower end of the range of values. However, a number of uncertainties need to be considered in making this comparison. The sea surface temperatures from the aircraft measurements listed in Table 4 are radiative skin temperatures, but the papers do not make it clear whether corrections have been made for the non-blackness of the sea surface (which would tend to reduce the values of C_{en}). The ship estimates are, in the main, based on temperatures measured below the surface, at depths ranging from a few centimetres to a few metres. Bradley *et al.* (1991) found that the difference between the water temperature at a depth of 2 m and the skin temperature was on average −0.3 degC in this region. For the typical values of the air–sea humidity difference, using the skin temperature would have increased their value of C_{en} by approximately 8%, which does not affect the agreement with the present results. In addition few of the authors in Table 4 state whether the effect of salinity on the saturation humidity at the sea surface is included (Bradley *et al.* (1991) and Fairall *et al.* (1996) do include it). Including the effect would increase estimates of C_{en} by about 6%.

The variability in the estimates in Table 4 is larger than the uncertainty in the C130 estimate indicated by the error bars in Fig. 3(c). This is because the error bars represent only the uncertainty in the estimates of the transfer coefficients due to random errors, primarily the sampling errors associated with the flux estimates (the larger error bars on the stress measurements in Fig 3(a) are consistent with the lower correlation coefficient between u and w compared with q and w). These error estimates do not represent the true uncertainty in C_{en}, as they do not include any estimate of the magnitude of systematic measurement errors.

The error in a single estimate of the moisture-transfer coefficient, C_e, can be written as,

$$\frac{\Delta C_e}{C_e} = \frac{\Delta wq}{wq} + \frac{\Delta U}{U} + \frac{\Delta Q}{(Q_{sea} - Q)} - \frac{\Delta Q_{sea}}{(Q_{sea} - Q)}, \tag{10}$$

where Δ represents the magnitude of the error in the appropriate quantity. Systematic differences between the C130 and *Franklin* humidity have been removed, to eliminate this element of uncertainty from the comparison with the COARE parametrization. However, the number of opportunities available to compare the C130 with the *Franklin* was small, and the uncertainty in the adjustments made to the C130 data can be taken to be at least as large as the accuracies quoted for the C130 and ship instruments. Based on these, an estimate of the possible systematic bias in C_{en} associated with errors in the mean measurements can be made.

Taking the uncertainties in the dew-point, sea surface temperature and winds given in section (*a*), Eq. (10) gives an overall uncertainty of $\approx 9\%$ for the C130 estimate of C_{en}. Fairall *et al.* (1996) list estimated accuracies for the *Moana Wave* bulk data which leads to an estimated uncertainty of 6% in C_{en}. These error estimates are similar to the variability in the values of C_{en} listed in Table 4 (assuming equal weights for each of the independent estimates). The difference between the *Moana Wave* and C130 estimates of C_{en} is $(0.18 \pm 0.10) \times 10^{-3}$, which is not significantly different from zero. This means that the difference between the C130 estimate of C_{en} and the COARE algorithm can be explained solely through errors in the mean measurements, and there is no evidence of a significant systematic difference in the flux measurements.

(*b*) *Area average turbulent fluxes*

Surface fluxes in large-scale numerical models, parametrized using Eqs. (2)–(4), use the grid point values for wind speed, air–sea temperature and humidity differences. For

TABLE 5. ESTIMATES OF THE GRID-AVERAGE LATENT-HEAT FLUX.

Flight	$< U >$ (m s^{-1})	Equation 11 (W m^{-2})	Equation 13 (W m^{-2})	Δ (W m^{-2})	$\sigma_s / < U >$
A224	3.1	62	75	13	0.53
A225	6.5	124	126	2	0.21
A232	4.3	90	106	16	0.30

the latent-heat flux this gives,

$$\lambda E_{\mathrm{mod}} = \rho \lambda C_e \overline{V}\ \overline{(Q_{\mathrm{sea}} - Q)}\,, \tag{11}$$

where the overbar denotes an average over a model grid box, and $\overline{V}$ is the vector averaged wind speed. However, because of subgrid fluctuations in the near-surface fields, the actual area averaged flux should more properly be estimated as

$$\lambda E_{\mathrm{act}} = \rho \lambda \overline{C_e U (Q_{\mathrm{sea}} - Q)} \tag{12}$$

where U is the scalar wind speed. In Eq. (12) it is assumed that the measurement height is sufficiently low for Eqs. (2) to (4) to hold at all points within the grid box. Equation (12) can be rewritten in terms of the grid box average and subgrid fluctuations as,

$$\lambda E_{\mathrm{act}} = \rho \lambda C_e \overline{U}\ \overline{(Q_{\mathrm{sea}} - Q)} + \rho \lambda C_e \overline{U'(Q_{\mathrm{sea}} - Q)'} \tag{13}$$

where the primes denote fluctuations with respect to the grid box average. In Eq. (13) variations in the transfer coefficient, C_e, associated with changes in stability and wind speed have been ignored. Young *et al.* (1995) have shown that variations in the transfer coefficients associated with convective outflows are relatively small (~15%).

The subgrid fluctuations can be seen to have two effects on the area averaged latent-heat flux. Firstly, there is an increase in the flux over that given by Eq. (11), because $\overline{U} > \overline{V}$. Secondly, correlations between the fluctuations in wind speed and the air–sea humidity difference can affect the area averaged flux. For the TOGA–COARE area, outflows from large convective clouds are a particularly significant source of subgrid-scale fluctuations. Changes in surface fluxes associated with such outflows can be large (e.g. Addis *et al.* 1984; Young *et al.* 1995), but it is difficult to assess the overall impact of the outflows on the area average flux from the published ship data. Aircraft measurements are better suited to investigating the effect of subgrid fluctuations on the area averaged surface flux.

The dimensions of the area covered by the C130 flights (150 × 150 km), are comparable to the dimensions of a grid square in a GCM. Table 5 lists estimates of the area average fluxes based on Eqs. (11) and (13) using averages over all the low-level runs on the three flights when convection was present. For C_e a typical flight-level value of 0.94×10^{-3} has been used. Wind speed, air and sea surface temperature and humidity used to calculate the area average flux with Eq. (11) were averaged over one kilometre. The increase in the flux due to subgrid fluctuations is up to 16 W m^{-2}, with the relative increase being larger at lower wind speeds. The increase is due mostly to the difference between the scalar and vector averaged wind speeds, the correlation term in Eq. (13) being negligible, at least for the present data. This is consistent with the results of Young *et al.* (1995), who analysed the change in the near-surface fluxes associated with convective outflows, and found that the changes in the latent-heat flux were largely due to changes in wind speed, systematic

changes in the air–sea humidity difference in the outflows being small. Jabouille *et al.* (1996) investigated the effect of convection on the surface flux using a cloud-resolving model. For a simulation of one day during the TOGA-COARE they found that the correlation term in Eq. (13) was small. Estimates of the enhancement due to gustinesss were similar to those found here. The estimates listed in Table 5 are relatively crude, and because the C130 avoided areas of intense rain, for safety reasons, they are also probably biased, but they suggest that the effect of subgrid-scale variability due to convective outflows on the area average surface flux is modest. There is also an enhancement of the area averaged sensible-heat flux of about 2 W m^{-2}. As with the humidity flux, this enhancement is due almost entirely to the gustiness, correlations between fluctuations in wind speed and the air–sea temperature difference being small.

In light winds, and in the absence of deep convective clouds, the latent-heat flux can be parametrized by including a gustiness factor associated with large convective eddies, which is proportional to the boundary-layer convective velocity-scale, $w_* = (g/\theta \overline{w\theta_v} z_i)^{1/3}$ (where z_i is the boundary-layer depth and $g/\theta \overline{w\theta_v}$ is the surface buoyancy flux), in the near-surface wind speed (Beljaars 1995). For the light wind conditions during the TOGA-COARE, $w_* \approx 0.6$ m s^{-1}; by comparison the standard deviation of the subgrid fluctuations in wind speed associated with convection was 1.5 m s^{-1} to 2.0 m s^{-1}. The enhancement of fluxes due to gustiness from deep convective clouds at low wind speeds is likely to be substantially larger than the enhancement due to boundary-layer gustiness alone.

Although Table 5 indicates that the effect of convective outflows on the area averaged fluxes are modest, this does not imply that convection does not have a significant effect on the turbulent fluxes at the surface. The presence of convection affects the low-level wind speed, temperature and humidity and it is these that ultimately determine the turbulent fluxes at the air–sea interface. This effect cannot be revealed by the present data.

(c) *The thermal balance of the boundary layer*

The sensible-heat flux is the smallest of the fluxes in the surface energy balance for all the flights listed in Table 3. However, it is significant for the thermal budget of the atmospheric mixed layer, since the flux divergence is equivalent to an increase in mixed-layer temperature of ≈1.5 degC day^{-1} in undisturbed conditions. Since this is comparable to the magnitude of the air–sea temperature difference, without a compensating cooling of the mixed layer to balance it, the sensible-heat flux would be expected to be even smaller, as the air–sea temperature difference would rapidly reduce to zero over a period of a day.

Table 6 lists estimates of the heating and cooling rates in the boundary layer due to the divergence of the turbulent flux $(= (\partial\theta/\partial t)_{\text{turb}})$ and long-wave radiative flux $(= (\partial\theta/\partial t)_{\text{lw}})$, for the four flights in undisturbed conditions. Under clear-sky conditions the long-wave cooling rate is approximately 0.1 K hr^{-1} which is similar to the long-wave cooling rates found by Nicholls and LeMone (1980) in the undisturbed GATE boundary layer. On average the magnitude of the long-wave cooling appears to be larger than the heating due to the turbulent flux divergence. For the three flights A227, A228 and A229 (for which cloud effects were small), there is a net cooling of approximately 0.05 K hr^{-1}. The presence of cloud on all of the flights makes it impossible to determine, directly from the pyranometer data, the heating rate due to short-wave absorption. However, the Edwards and Slingo (1996) radiation scheme, together with aircraft profiles, gives a daily averaged heating rate in the boundary layer of 0.03 degC hr^{-1}, neglecting any possible absorption due to aerosols. During the daylight hours the solar heating is larger than the average, being approximately 0.06 degC hr^{-1}. This heating rate is comparable to the imbalance between the sensible-heat flux divergence and the long-wave cooling, indicating that under these

TABLE 6. TERMS IN THE THERMAL BALANCE OF THE BOUNDARY LAYER.

Flight Number	$(\partial\theta/\partial t)_{\text{turb}}$ (K hr^{-1})	$(\partial\theta/\partial t)_{\text{lw}}$ (K hr^{-1})
A227	+0.047	−0.119
A228	+0.089	−0.096
A229	+0.059	−0.129
A233	+0.053	−0.051

$(\partial\theta/\partial t)_{\text{turb}}$ is the rate of change of temperature due to the turbulent flux and $(\partial\theta/\partial t)_{\text{lw}}$ is the change due to the long-wave flux.

undisturbed conditions there is a balance between the turbulent and radiative fluxes on a daily time-scale.

The close balance between turbulent and radiative heating rates means that the diurnal variation in the heating due to solar absorption should lead to a corresponding diurnal variation in the mixed-layer temperature. Such a variation would be in addition to any diurnal variations in the sea surface temperature. Assuming the solar heating rate can be represented by a periodic top-hat function, with a non-zero value for 12 hours, the maximum variation in the air–sea temperature difference will be

$$\Delta T_{\max} = \frac{Sh}{C_{\text{h}}U}\,, \tag{14}$$

where S is the solar heating rate during daylight hours; h is the mixed layer depth; C_{h} is the transfer coefficient for sensible heat; and $\Delta T_{\max}$ is the diurnal variation in air–sea temperature difference.

The time-scale $h/(C_{\text{h}}U)$ represents the time for the mixed layer to respond to changes in the radiative forcing. For $U = 4$ m s^{-1} and $h = 700$ m the time-scale is 35 hours, significantly longer than the period of solar heating. Hence the actual diurnal change in temperature will be smaller than given by Eq. (14), and should be approximately,

$$\Delta T = \Delta T_{\max}(1 - \exp(-C_{\text{h}}Ut_{1/2}/h)) \tag{15}$$

where $t_{1/2}$ is twelve hours. Taking S to be 0.06 degC hr^{-1} the diurnal change in air temperature due to solar heating is about 0.5 degC. The magnitude of this variation is insensitive to wind speed. Zhang (1995) found that the air temperature measured by the IMET buoy showed a clear diurnal variation under clear-sky conditions, even with high wind speeds (when the diurnal variation in sea surface temperature is small). Zhang (1995) and Chen and Houze (1997) suggest that the diurnal cycle of temperature in the mixed layer may play a role in the diurnal variation of deep convection, particularly for the smaller scale convective systems.

Betts and Ridgeway (1988) argued that, climatologically, the surface sensible- and latent-heat fluxes are closely coupled to the radiative fluxes and large-scale subsidence, although in the climatological context clouds play an important role.

(*d*) *Radiative fluxes*

The downwelling short-wave flux is generally the largest and most variable term in the surface energy balance, and it is consequently important that it should be parametrized

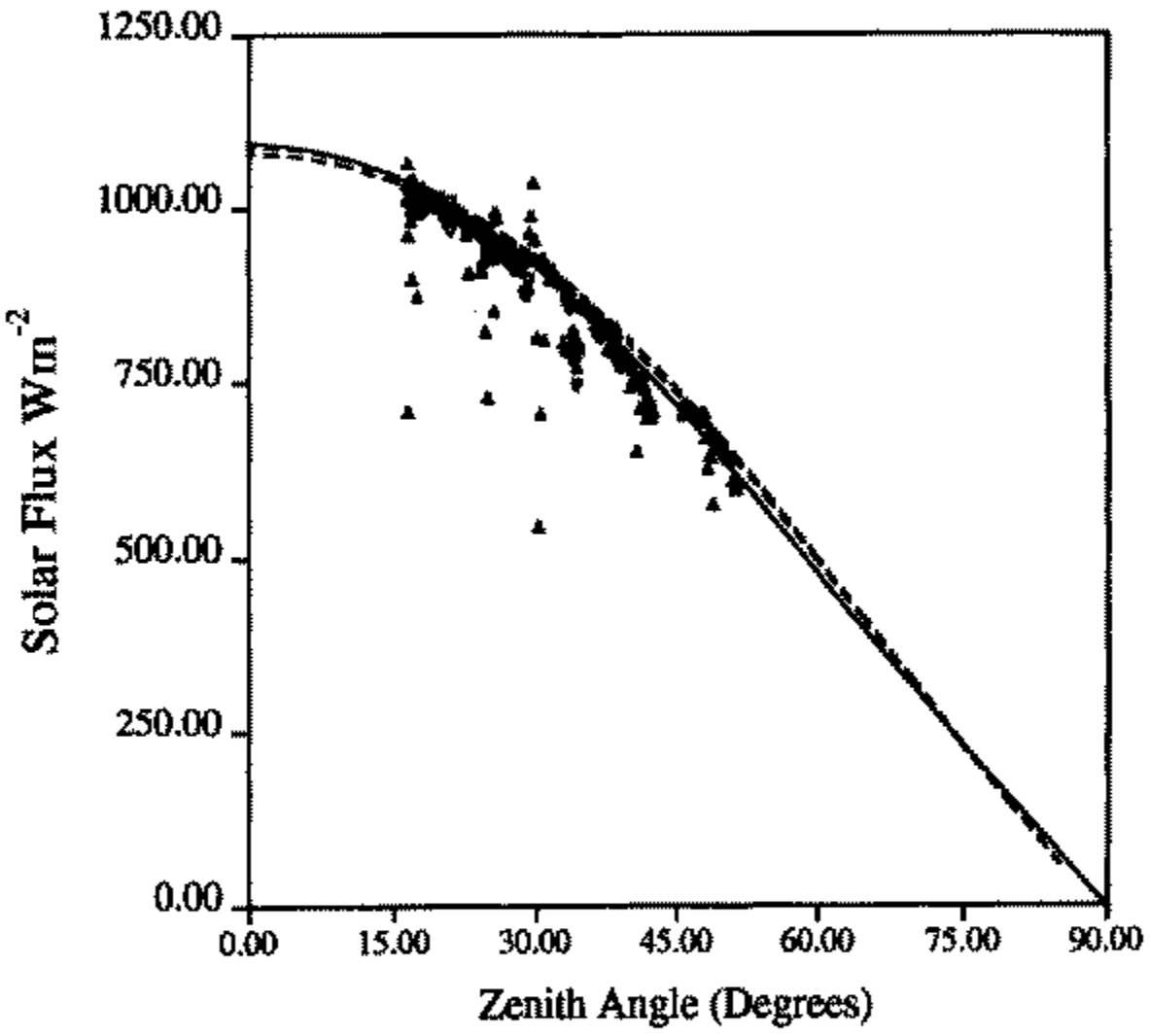

Figure 4. Solar fluxes observed on flights A227, △, and A228, ▽. The dashed curves are fluxes calculated using the Edwards and Slingo (1996) model for the two flights, and the full curve the parametrization of Lumb (1964).

accurately. For surface energy balance studies relatively simple parametrizations involving sun zenith angle and cloud amounts are appropriate, and such parametrizations are considered below. In GCMs the surface radiative fluxes are usually calculated from a radiation scheme, together with assumptions concerning cloud optical properties and geometries. Whilst the simpler parametrizations considered here may not be appropriate to GCMs, they provide scope for evaluating the more complicated GCM parametrizations for complex cloud ensembles.

Lumb (1964) obtained a parametrization for clear-sky solar fluxes from weather ship observations which is compared with the data from flights A227 and A228 and the explicit calculations using the Edwards and Slingo model in Fig. 4. The Lumb parametrization was developed using data collected in the north Atlantic, and the agreement with the present data is very good. The agreement with the Edwards–Slingo scheme is also good. The scatter in the observed fluxes is caused by the small amount of cumulus cloud present on these days. The points that lie above the curves are due to the enhancement of the solar flux by reflection from the sides of the clouds.

The fraction of the expected clear-sky flux that arrives at the surface is largely controlled by cloud cover. Visual cloud observations were made during the C130 flights by the aircraft scientist, but it is difficult to combine these observations into a representative cloud cover over a 150 km horizontal flight leg. A more representative estimate of the cloud amount can be obtained from the output of the upward facing pyranometer, by calculating the fraction of the record for which the observed solar flux is less than the calculated clear-sky flux by some specified amount. Figure 5 shows the ratio between the observed solar flux and the clear-sky flux, $S^{\downarrow}_{\mathrm{obs}}/S^{\downarrow}_{\mathrm{clear}}$, as a function of cloud amount, N (the aircraft was assumed to be passing through a cloud shadow if the measured flux was less than the clear-sky flux calculated from Lumb's parametrization by more than 30 W m^{-2}).

The reduction of solar radiation as a function of cloud fraction is not linear, and the ratio $S^{\downarrow}_{\mathrm{obs}}/S^{\downarrow}_{\mathrm{clear}}$ remains close to unity for cloud fractions less than 0.4. At these low cloud fractions the solar flux, which is that through a horizontal surface, is enhanced relative to the equivalent plane-parallel cloud, by reflections from cloud sides. Two parametrizations

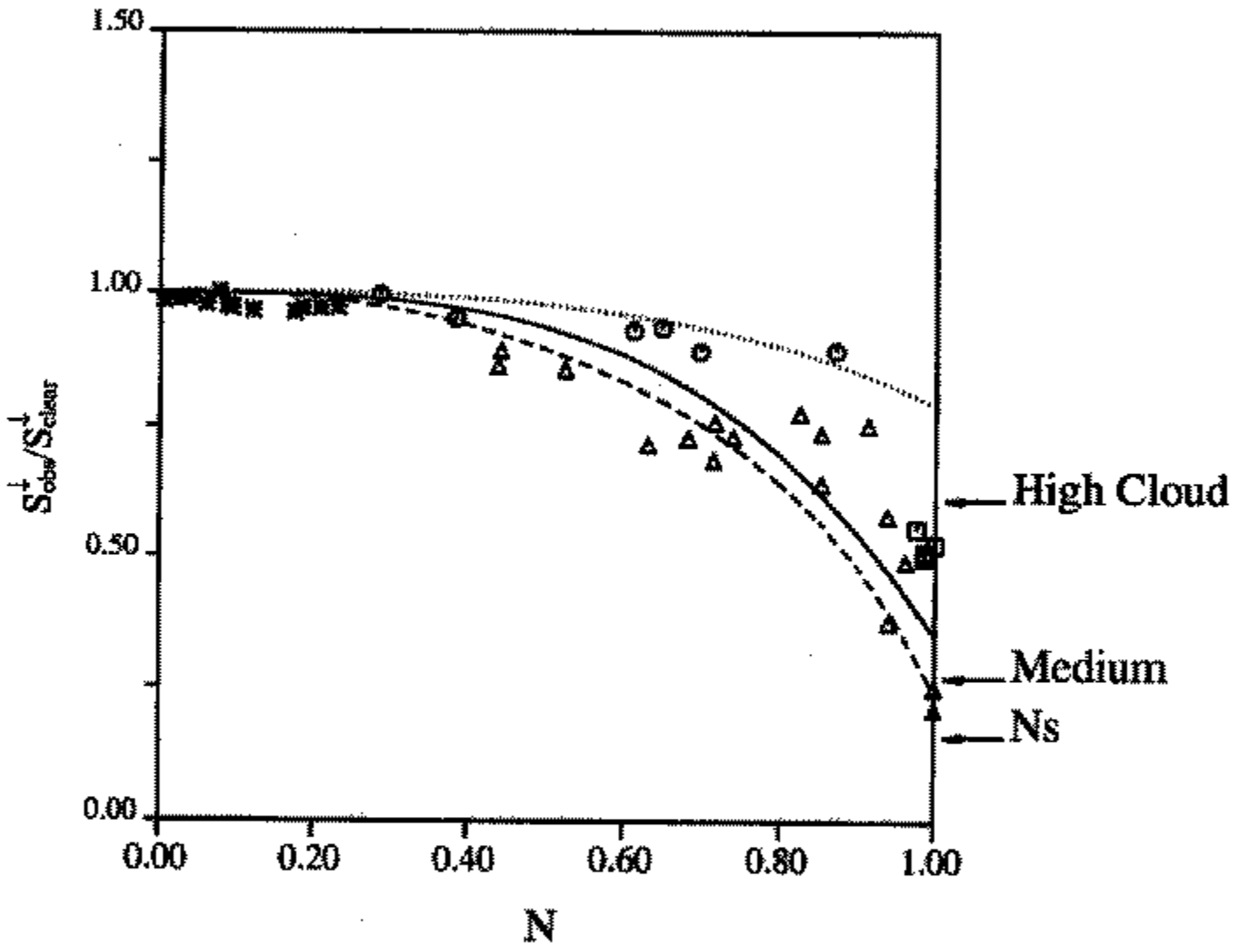

Figure 5. Cloud transmittance as a function of cloud amount, N. Small cumulus, ∗, deep convection and mid-layer cloud △, cirrus, ◯. Curves are parametrizations due to Kasten and Czeplak (1980) (full curve), Kondo and Miura (1985) for low cloud only (dashed curve) and high cloud only (dotted curve). The arrows along the right-hand edge are transmittances from Kasten and Czeplak (1980) for full cover of different cloud types.

are compared with the aircraft data in Fig. 5. One is due to Kasten and Czeplak (1980) based on data collected in Hamburg:

$$\frac{S^{\downarrow}_{\text{obs}}}{S^{\downarrow}_{\text{clear}}} = 1 - AN^{3.4}\,, \tag{16}$$

where N is the total cloud fraction and A is a constant. The second parametrization is due to Kondo and Miura (1985) and was obtained using data from the monsoon experiment, MONEX, which took place in the equatorial west Pacific, and consequently might be considered to be more representative of the present data:

$$\frac{S^{\downarrow}_{\text{obs}}}{S^{\downarrow}_{\text{clear}}} = 0.836 + 0.521(C - 0.4\mathrm{e}^{-3C_1}) + 0.737\ln\{1.22 - 1.02(C - 0.4\mathrm{e}^{-3C_1})\}\,, \tag{17}$$

where C is the total cloud amount and C_1 is the amount of low cloud. Two curves are shown for this parametrization, one for which all the cloud is assumed to be low cloud, and the second which assumes no low cloud is present.

Both parametrizations appear to give a good representation of the present data for low and medium cloud. The present data are consistent with $A = 0.65$ in Eq. (16), which is similar to the value found by Kasten and Czeplak (1980). They also found that the reduction in incoming solar radiation for full cloud cover depended on cloud type, and these results are marked along the side of Fig. 5. Their estimate for the attenuation due to cirrus appears to be rather larger than the limited aircraft data suggest, which probably reflects the different origins of cirrus. In midlatitudes most cirrus is associated with fronts, whilst the cirrus in the present data came from convective systems. Equation (17) with $C_1 = 0$ is in much better agreement with the present aircraft data obtained under cirrus.

The net long-wave flux is a much smaller term in the surface energy balance than the net solar flux, but the magnitudes of the downwelling short-wave and long-wave radiative

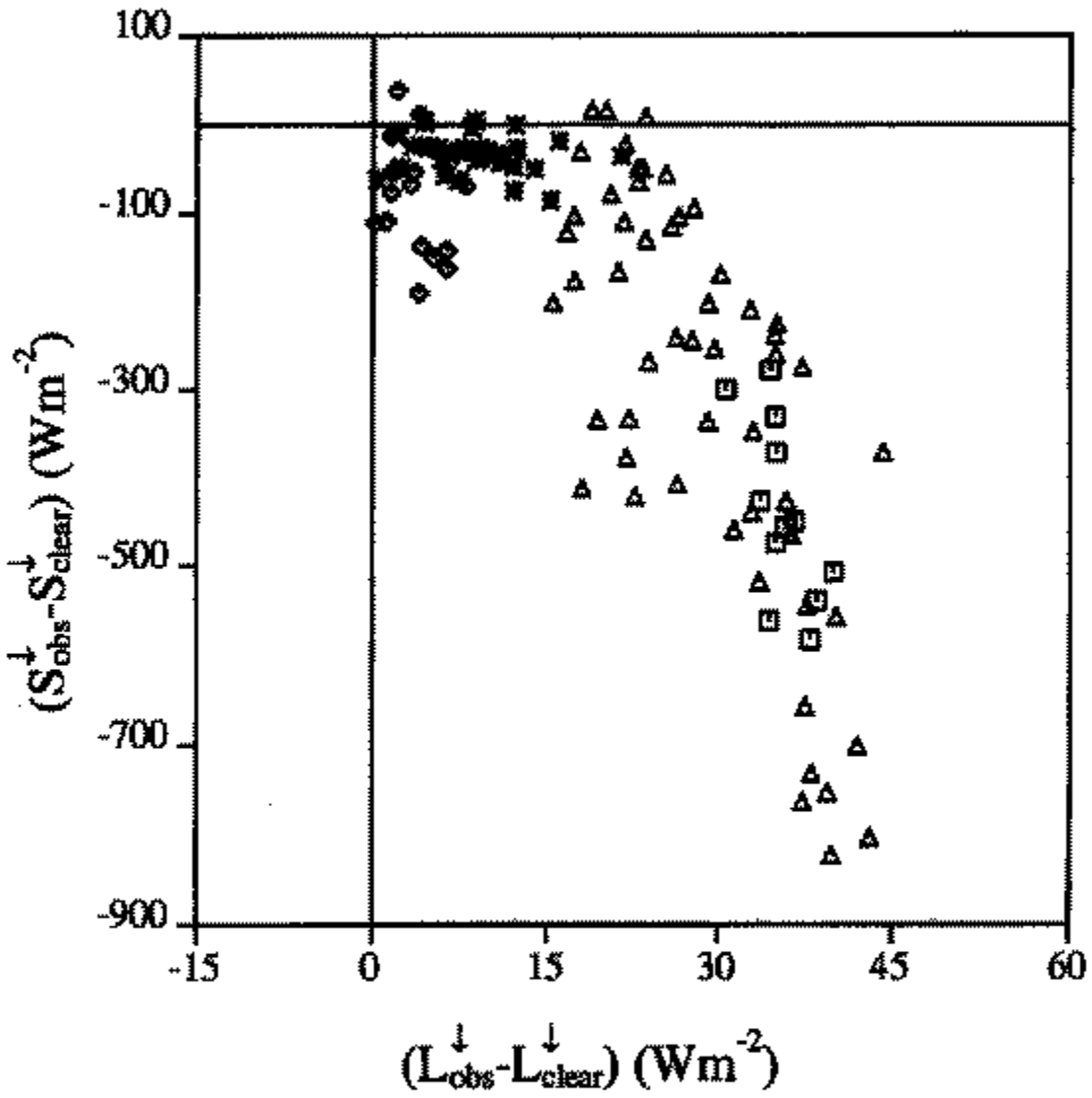

Figure 6. Short-wave cloud forcing versus long-wave cloud forcing (see text). Symbols: ◇, Cirrus cloud; ∗, Small cumulus; △, Deep cumulus; □, Stratiform cloud.

fluxes are correlated. Figure 6 shows a plot of the short-wave cloud forcing ($S^{\downarrow}_{\text{obs}} - S^{\downarrow}_{\text{clear}}$) against the long-wave cloud forcing ($L^{\downarrow}_{\text{obs}} - L^{\downarrow}_{\text{clear}}$). The observed fluxes have been calculated as averages over 25 km. The clear-sky short-wave flux was calculated as before using the Edwards–Slingo radiation model. The clear-sky long-wave flux was estimated from cloud-free sections of the aircraft track. The long-wave fluxes obtained in this manner varied by only ± 5 W m^{-2}, and for flights in which no clear-sky data were available an average value of $L^{\downarrow}_{\text{clear}}$ was used.

The effects of different cloud types and conditions on the radiative balance at the surface can be seen in Fig. 6. With mainly cirrus cloud cover (represented by the diamond symbols) there is a modest short-wave forcing but, because of the high cloud base (typically >10 km), only a small impact on the long-wave forcing. By contrast small cumulus (crosses), with bases at ≈600 m, have a significant effect on the long-wave forcing but, because the downward short-wave flux at the surface is enhanced by reflection from the cloud sides, there is little impact on the short-wave forcing. Deep convective clouds (triangles) and extensive medium-level layer cloud (squares) have a substantial effect on both fluxes. In the presence of deep convective cloud the variability in short-wave forcing is very large because of the three-dimensional cloud field. Reflections from cloud sides cause enhanced short-wave fluxes at the surface in some areas, while deep shadows lead to a large reduction in the flux in others.

Figure 7 shows the average cloud forcing for each of the flights. The measured short-wave forcing has been used to estimate a daily averaged forcing as described above. For the conditions covered by the C130 flights there is a clear relationship between the estimated daily averaged short-wave and long-wave cloud forcings. For a reduction of 150 W m^{-2} in the short-wave flux the downwelling long-wave flux increases by approximately 30 W m^{-2}. Also shown in Fig. 7 are cloud forcings calculated from the IMET buoy. These data cover the whole of the COARE intensive observing period and a wider range of conditions than the C130 data, which was restricted to periods with generally unorganized convection. For the IMET data the clear-sky short-wave flux was calculated as above and the clear-sky

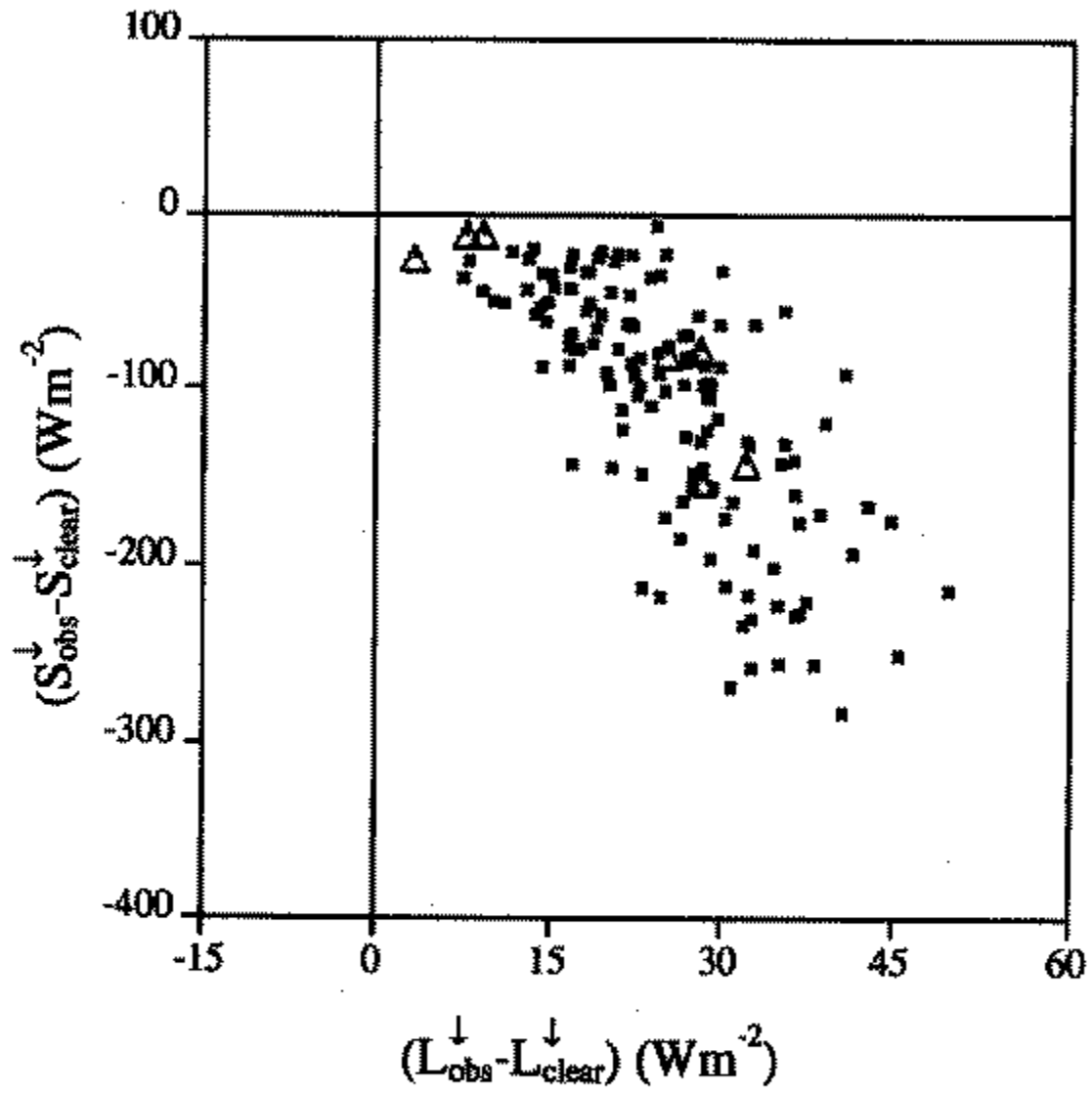

Figure 7. Comparison between daily averaged radiative cloud forcing from the IMET buoy, ∗, and the C130, △; see text.

long-wave flux estimated simply by fitting, by eye, a Brunt-type expression to the data, i.e.

$$L^{\downarrow} = \sigma T_{\text{air}}^{4}(a + bq_{\text{air}}^{1/2}) \tag{18}$$

The values of a and b are 0.24 and 4.33, respectively, with the humidity, q, in kg kg^{-1}. Arnfield (1979) noted that published values for the coefficients a and b in Eq. (18) are very variable, and the present values differ from the average value obtained from Arnfield's Table 1. However, using the average values of a and b from Arnfield (1979) gives an estimate of the downwelling long-wave flux that differs by only 10 W m^{-2} from those obtained with the above values, a difference that is within the uncertainty of the measured long-wave fluxes. The relationship between the short-wave and long-wave cloud forcing derived from the IMET buoy data is similar to that obtained from the more restricted aircraft data set. On about 25% of days the IMET buoy data show short-wave forcings that are considerably larger than observed by the C130. Presumably these represent the effect of the larger mesoscale convective systems that affect the TOGA-COARE area. The variation in the long-wave forcing is similar to that obtained from the aircraft data.

4. Conclusions

This paper has presented some aspects of the surface energy balance of the Pacific warm pool region, using data collected by an instrumented aircraft. The observations were obtained under undisturbed and moderately disturbed conditions. No data were obtained in the presence of mesoscale convective systems, which are a significant feature of the region.

The dominant, and most variable terms, of the surface energy balance were the solar and latent-heat fluxes. Of the seven flights considered six gave a net energy flux of about 60 W m^{-2} into the ocean, whilst the remaining flight gave a net energy loss. Conditions

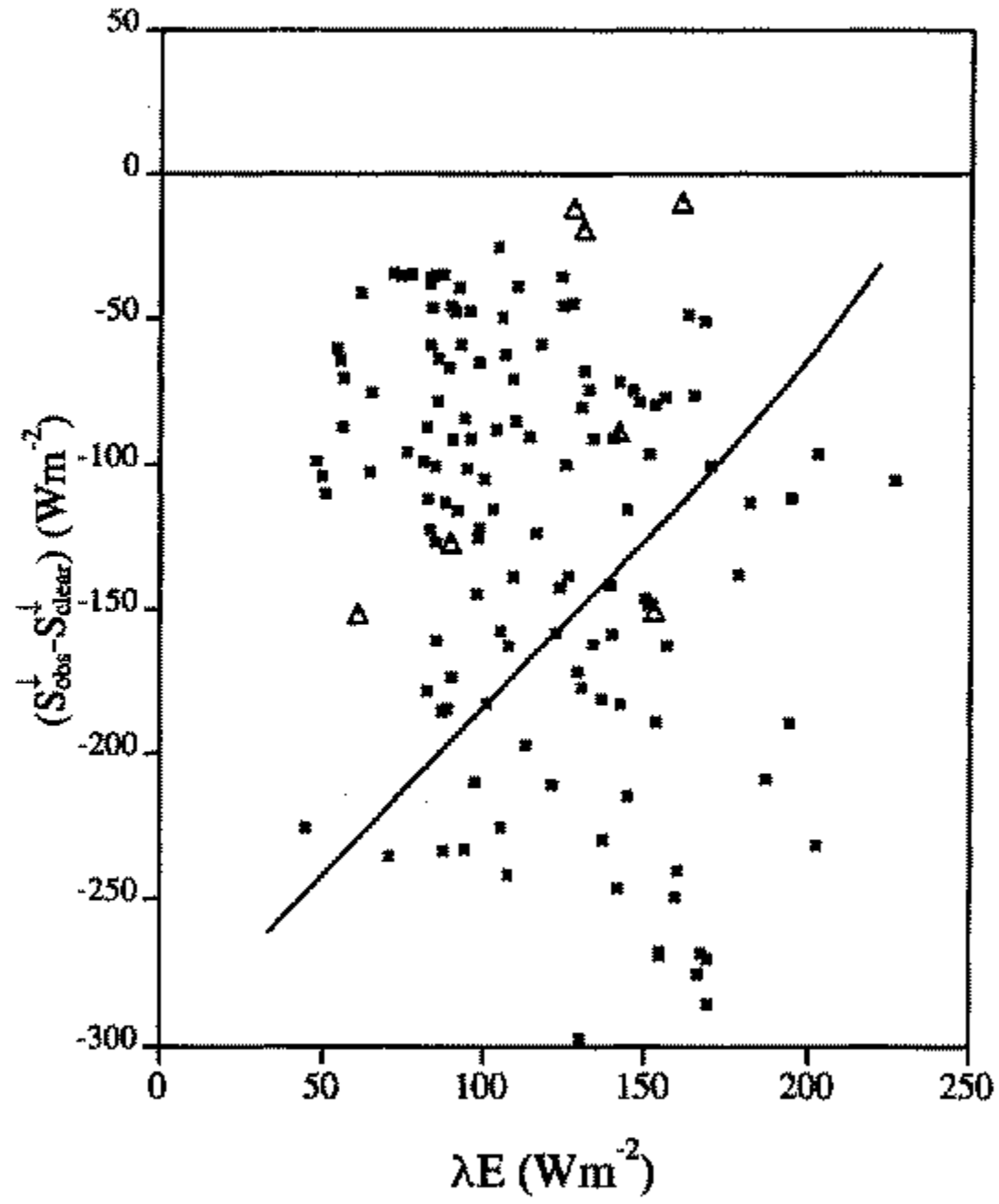

Figure 8. Plot of the daily averaged short-wave cloud forcing ($S^{\downarrow}_{obs} - S^{\downarrow}_{clear}$) against the daily average latent-heat flux (λE) from the IMET buoy (∗). The line denotes a net energy flux of zero and the triangles are the data from the C130.

on the latter day were overcast and windy, mid-level cloud originating from a convective system to the south of the aircraft operating area reducing the solar flux at the surface.

The neutral transfer coefficient for moisture obtained from the aircraft data was 0.93×10^{-3}, which is within the range of published values obtained over the tropical oceans, but lower than the value obtained from the *Moana Wave* during the TOGA-COARE. However, the magnitudes of possible systematic biases in the mean data used in calculating the transfer coefficients is between 5% and 10%, so that the difference between the C130 and *Moana Wave* is not significant. There is no evidence from this study that the airborne and ship flux data show any significant difference. As more data become available from the other flux measuring platforms it should become possible to obtain a more accurate value for the transfer coefficient.

For the aircraft flights in disturbed conditions the C130 data suggest enhancements of the latent-heat flux of up to 16 W m^{-2} due to gustiness in the wind associated with convective outflows. The correlation between the wind and humidity in outflows does not appear to lead to any significant enhancement in the area-averaged flux.

In undisturbed conditions, the data suggest that over the mixed layer the turbulent flux divergence balances the net radiative cooling. The estimated heating due to the absorption of solar radiation by water vapour appears to be a significant term in the balance. The diurnal variation in the solar heating should lead to a corresponding variation in the mixed-layer temperature. The amplitude of such a variation is estimated to be about 0.5 degC. Because the response time of the mixed layer to changes in the solar absorption depends on wind speed, the amplitude of this diurnal variation is almost independent of wind speed. Although for the cases considered convection was not present, such diurnal variations in the mixed-layer temperature may play an important role in the diurnal modulation of convection in the warm pool region (Chen and Houze 1997).

The reduction in the area averaged downwelling solar flux by clouds obtained here agrees well with other simple parametrizations based on cloud amounts. In particular, a parametrization for cirrus cloud obtained from MONEX data was in good agreement with the aircraft data. Downwelling solar and long-wave radiative fluxes are correlated, with the particular form of the correlation depending on the cloud type.

The aircraft data presented here are clearly not representative of the average energy balance of the region. Figure 8 shows a plot of daily averaged short-wave cloud forcing and latent-heat fluxes from the IMET buoy and the C130. The line in the figure shows a net flux of zero (taking the relationship between solar and long-wave fluxes from Fig. 7 and assuming a sensible-heat flux of 10 W m^{-2}). Over the longer period covered by the IMET buoy data there is an even split between periods of energy loss from the ocean and energy gain. The restricted nature of the aircraft data are apparent in this plot, particularly the lack of measurements with large short-wave cloud forcing.

Acknowledgements

We would like to thank the staff and aircrew of the Meteorological Research Flight and the staff of the TOGA-COARE International Project Office without whose efforts this work would not have been possible. The data from the IMET buoy were provided by Dr Robert Weller of the Woods Hole Oceanographic Institute and the *Franklin* data by Frank Bradley and Peter Coppin of the CSIRO Centre for Environmental Mechanics. We would also like to acknowledge the useful suggestions and comments made by the two anonymous referees.

References

Addis, R. P., Garstang, M. and Emmitt, G. D. 1984 Downdrafts from tropical oceanic cumuli. *Boundary-Layer Meteorol.*, **28,** 23–50

Arnfield, A. J. 1979 Evaluation of empirical expressions for the estimation of hourly and daily totals of atmospheric longwave emission under all sky conditions. *Q. J. R. Meteorol. Soc.*, **105,** 1041–1052

Beljaars, A. C. M. 1995 The parametrization of surface fluxes in large scale models under free convection. *Q. J. R. Meteorol. Soc.*, **121,** 255–270

Berk, A., Bernstein, L. S. and Robertson, D. C. 1989 'MODTRAN: A moderate resolution model for LOWTRAN7.' Report AFGL-TR-89-0122, US Air Force Geophysics Laboratory, Hanscomb AFB, MA, USA.

Betts, A. K. and Ridgway, W. 1988 Coupling of the radiative, convective and surface fluxes over the equatorial Pacific. *J. Atmos. Sci.*, **45,** 522–536

Bradley, E. F. and Weller, R. A. (editors) 1995 Third workshop of the TOGA-COARE air sea interaction (flux) working group, 2–4 August 1995. University of Hawaii, Honolulu, USA. (TOGA-COARE International project office, University Corporation for Atmospheric Research, Boulder USA).

Bradley, E. F., Coppin, P. A. and Godfrey, J. S. 1991 Measurements of sensible and latent heat flux in the western equatorial Pacific ocean. *J. Geophys. Res.*, **96,** 3375–3389

Buck, A. L. 1981 New equations for computing vapour pressure and enhancement factor. *J. Appl. Meteorol.*, **20,** 1527–1532

Chen, S. S. and Houze, R. A. 1997 Diurnal variation and life cycle of deep convective systems over the tropical Pacific warm pool. *Q. J. R. Meteorol. Soc.*, **123,** 357–388

Coantic, M. and Friehe, C. A. 1980 Slow response humidity sensors. In *Air–sea interaction, Instruments and methods*. Eds. F. Dobson, L. Hasse and R. Davis, Plenum Press, New York

Edwards, J. M. and Slingo, A. 1996 Studies with a flexible new radiation code I: Choosing a configuration for a large-scale model. *Q. J. R. Meteorol. Soc.*, **122,** 689–720

Ellingson, R. G., Ellis, J. and Fels, S. 1991 The intercomparison of radiation codes used in climate models: Longwave results. *J. Geophys. Res.*, **96,** 8929–8953

Fairall, C. W., Bradley, E. F., Rogers, D. P., Edson, J. B. and Young, G. S. 1996 Bulk parametrisation of air–sea fluxes for TOGA-COARE. *J. Geophys. Res.*, **101,** 3744–3764

Foot, J. S. 1986 A new pyrgeometer. *J. Atmos. Oceanic Technol.*, **3,** 363–370

Friehe, C. A., Grossman, R. L. and Penn, Y. 1986 Calibration of an airborne Lyman-alpha hygrometer and measurement of water vapor flux using a thermo-electric hygrometer. *J. Atmos. Oceanic Technol.*, **3,** 299–304

Fujitani, T. 1992 Turbulent transport mechanism in the surface layer over the tropical ocean. *J. Meteorol. Soc. Jpn.*, **70,** 795–810

Gordon, C. and Corry, R. A. 1991 A model simulation of the seasonal cycle in the tropical Pacific ocean using climatological and modelled surface forcing. *J. Geophys. Res.*, **96,** 847–864

Greenhut, G. K. and Bean, B. R. 1981 Aircraft measurements of boundary layer turbulence over the central equatorial Pacific ocean. *Boundary-Layer Meteorol.*, **20,** 221–242

Greenhut, G. K. and Khalsa, S. J. S. 1995 Bulk transfer coefficients and dissipation derived fluxes in low windspeed conditions over the western equatorial Pacific ocean. *J. Geophys. Res.*, **100,** 857–863

Hogstrom, U. 1988 Non-dimensional wind and temperature profiles in the atmospheric surface layer: a re-evaluation. *Boundary-Layer Meteorol.*, **42,** 55–78

Hosom, D. S., Weller, R. A., Payne, R. E. and Prada, K. E. 1995 The IMET (Improved Meteorology) ship and buoy system. *J. Atmos. Oceanic Technol.*, **12,** 527–540

Jabouille, P., Redelsperger, J.,-L. and Lafore, J. P. 1996 Modification of surface fluxes by atmospheric convection in the TOGA-COARE region. *Mon. Weather Rev.*, **124,** 816–837

Kaimal, J. C. 1986 Flux profile measurements from towers in the boundary layer. Pp. 19–28 in *Probing the atmospheric boundary layer*, Ed. D. H. Lenschow. American Meteorological Society, Boston, USA

Kasten, F. and Czeplak, G. 1980 Solar and terrestrial radiation dependent on the amount and type of cloud. *Solar Energy*, **24,** 177–189

Kondo, J. and Miura, A. 1985 Surface heat budget of the western Pacific for May 1979. *J. Meteorol. Soc. Jpn.*, **63,** 633–646

Kraus, E. B. 1972 *Atmosphere–ocean interaction*. Clarendon Press, Oxford, UK

Liu, W. T., Katsaros, K. B. and Businger, J. A. 1979 Bulk parameterisation of air–sea exchange of heat and water vapor including molecular constraints at the interface. *J. Atmos. Sci.*, **36,** 1722–1735

Lumb, F. E. 1964 The influence of cloud on hourly amounts of total solar radiation at the sea surface. *Q. J. R. Meteorol.*, **90,** 43–56

Mann, J. and Lenschow, D. H. 1994 Errors in airborne flux measurements. *J. Geophys. Res.*, **99,** 14519–14526

McCarthy, J. 1973 A method for correcting airborne temperature data for sensor response time. *J. Appl. Meteorol.*, **12,** 211–214

Nicholls, S. 1978 Measurements of turbulence by an instrumented aircraft in a convective atmospheric boundary layer over the sea. *Q. J. R. Meteorol. Soc.*, **104,** 653–676

Nicholls, S. and LeMone, M. A. 1980 The fair weather boundary layer in GATE: The relationship of subcloud fluxes and structure to the distribution and enhancement of cumulus clouds. *J. Atmos. Sci.*, **37,** 2051–2067

Nicholls, S., Leighton. J. and Barker, R. 1990 A new fast response instrument for measuring total water content from aircraft. *J. Atmos. Oceanic Technol.*, **7,** 706–718

Nicholls, S., Shaw, W. and Hauf, T. 1983 An intercomparison of aircraft turbulence measurements made during JASIN. *J. Appl. Meteorol.*, **22,** 1637–1648

Saunders, P. M. 1970 Corrections for airborne radiation thermometry. *J. Geophys. Res.*, **75,** 7596–7601

Saunders, R. W., Brogniez, G., Buriez, J. C., Meerköter, R. and Wendling, P. 1992 A comparison of measured and modelled broadband fluxes from aircraft data during the ICE '89 field experiment. *J. Atmos. Oceanic Technol.*, **9,** 391–406

Smith, S. D. 1989 Water vapor flux at the sea surface. *Boundary-Layer Meteorol.*, **47,** 277–293

Song, X., Friehe, C. A. and Hu, D. 1996 Shipboard measurements and estimations of air–sea fluxes in the western tropical Pacific during TOGA-COARE. *Boundary-Layer Meteorol.*, **81** 373–397

Tsukamoto, O. and Ishuda, H. 1995 Turbulent flux measurements and energy budget analysis over the equatorial Pacific during TOGA-COARE IOP. *J. Meteorol. Soc. Jpn.*, **73,** 557–568

WCRP 1990 'Scientific plan for the TOGA Coupled Ocean–Atmosphere Response Experiment'. In addendum to World Climate Research Program Publication Series, No. 3, WMO, Geneva

Webster, P. J. and Lukas, R. 1992 TOGA-COARE: The coupled ocean atmosphere response experiment. *Bull. Amer. Meteorol. Soc.*, **73,** 1377–1416

Young, G. S., Perugini, S. M. and Fairall, C. W. 1995 Convective wakes in the equatorial Pacific during TOGA. *Mon. Weather Rev.*, **123,** 110–123

Zhang, C. 1995 'The diurnal cycle in surface air temperature in the western Pacific warm pool region'. Pp 494–498 in Proceedings of the international scientific conference on the TOGA programme, 2–7 April 1995, Melbourne, Australia. WMO/TD No. 7171 Vol. I

Zhang, G. J. and Grossman, R. L. 1996 Surface evaporation during the Central Equatorial Pacific Experiment: A climate scale perspective. *J. Climate*, **9,** 2522–2537